Chemical Engineering Journal 445 (2022) 136653

Contents lists available at ScienceDirect

Chemical Engineering Journal

journal homepage: www.elsevier.com/locate/cej

Drag correlations for flow past monodisperse arrays of spheres and porous spheres based on symbolic regression: Effects of permeability

Likun Ma [a,b], Qiang Guo [c], Xue Li [d], Shuliang Xu [a], Jibin Zhou [a], Mao Ye [a,*], Zhongmin Liu [a,b]

[a] Dalian National Laboratory for Clean Energy and National Engineering Laboratory for MTO, Dalian Institute of Chemical Physics, Chinese Academy of Sciences, Dalian 116023, China
[b] University of Chinese Academy of Sciences, Beijing 100049, China
[c] Department of Chemical Engineering, Columbia University, New York 10027, United States
[d] State Key Laboratory of Catalysis, Dalian Institute of Chemical Physics, Chinese Academy of Sciences, Dalian 116023, China

ARTICLE INFO

Keywords:
Drag correlation
Permeability
Symbolic regression
Porous sphere
Monodisperse arrays of spheres

ABSTRACT

An accurate drag correlation accounting for multiscale heterogeneous porous structures is a prerequisite for reliable CFD simulation of fluidized beds. Though particle clusters in fluidized beds are usually modeled as porous particles, particle-resolved direct numerical simulation (PR-DNS), in which monodisperse arrays of spheres are taken as model systems, has been widely used as a first-principle approach to derive drag correlations. This work is to bridge the gap of drag correlations for monodisperse arrays of spheres and porous spheres by considering permeability effects and derive new drag correlations using symbolic regression (SR) methods. Firstly, experimental porous spheres settling data were utilized to identify the most important features affecting drag force using Support Vector Machine (SVM), in which the permeability β was packed up in addition to the solid fraction ϕ and Reynolds numbers Re. A new drag correlation for porous spheres based on ϕ,Re, and β, which has physical terms, high prediction accuracy and correct limiting cases, is automatically generated using SR method. Then, PR-DNS data from open sources were used to distill drag correlations for monodisperse arrays of spheres by incorporating the extra permeability parameter by SR method, demonstrating solid physical basis with high accuracy. It is further shown the SR based on drag correlations for porous spheres and monodisperse arrays of spheres can be reduced to limiting cases of a single solid sphere and Stokes flow. The proposed new drag correlations not only provide a way to use permeability as a simple yet physically sounded parameter to quantify heterogeneous structures in fluidized beds, but also open a venue for directly validating drag correlations obtained purely from PR-DNS simulations with experimental data of flow around porous spheres.

1. Introduction

Porous structures are widely encountered in industrial processes and two particular and essential examples are fixed/packed bed reactors [1–3] and particle clusters or agglomerates in fluidization systems [4,5]. Fixed bed reactors, defined as an assembly of particles, are usually regular/random packings of uniformly sized spheres [1]. Particle clusters or agglomerates in fluidization systems are usually modeled as porous spheres [6,7]. To gain a better design and optimal control of these industrial processes which manifests porous structures, it is essential to accurately describe the hydrodynamics therein [8]. CFD simulations are playing an increasingly important role in this regard. At industrial scale, CFD simulations are mainly based on the Euler–Euler or Euler-Lagrange models, both of which require in prior drag correlations as input to account for the gas-particle interactions [9]. An accurate drag correlation derived via either well-designed experiments or first-principle simulations, is a prerequisite in obtaining reliable CFD simulation results [10–13]. Essentially, the choice of drag correlations, especially the formula forms used, can significantly affect the numerical simulation results [14–17]. Thus, it's necessary to obtain accurate drag correlations for above porous systems.

It should be noted that in this work, drag force F_d due to the friction between particle and fluid phase was used by converting all collected total force $F_{g\to s}$ that the fluid exerts on the solid particles to F_d [18]. In addition, F_d is normalized by the Stokes drag force for an isolated particle [19], which is written as dimensionless drag force $F(\phi, Re) =$

* Corresponding author.
E-mail address: maoye@dicp.ac.cn (M. Ye).

https://doi.org/10.1016/j.cej.2022.136653
Received 4 January 2022; Received in revised form 26 March 2022; Accepted 26 April 2022
Available online 4 May 2022

$F_d/3\pi\mu du$.

For monodisperse arrays of spheres systems, at the limit of $Re \sim 0$, the most representative drag correlation is Carman-Kozeny (CK) relation, which is written as $F = 2k \times \phi/(1-\phi)^2$ and can be theoretically derived based on the assumption of stokes flow through a monodisperse dense random array of spheres [20]. The Carman theoretical term $2k \times \phi/(1-\phi)^2$ was considered as a basic term in the subsequent development of drag correlations. For instance, assuming $k = 5$ can reduce the CK relation to the Carman equation [21] and assuming $k = 4.167$ can further reduce it to the Ergun equation [21]. In the work by van der Hoef et al. [21], they added an extra term $(1-\phi)^2(1+1.5\sqrt{\phi})$ into the Carman equation to obtain the correct limit of $F \to 1$ at $\phi \to 0$. Up to now, $F = 10\phi/(1-\phi)^2 + (1-\phi)^2(1+1.5\sqrt{\phi})$ proposed by van der Hoef et al. [21] is still the most accurate drag correlation for flows of $Re \sim 0$ which indicates drag force F is solely related to solid fractions ϕ for $Re \sim 0$, making them "one-maker" drag models. For flows with finite Reynolds number ($Re > 0$), there are two commonly used formula forms [9]. The first one is the Ergun-type equation $F(\phi, Re) = F(\phi, 0) + \alpha Re$ which is based on drag force of Stokes flow $F(\phi, 0)$ at $Re = 0$ with an addition linear term α on Re to account for the effects of inertia at $Re > 0$. The second one is the Wen & Yu-type equation $F(\phi, Re) = F(0, Re)(1-\phi)^{-\beta}$ which is based on drag force $F(0, Re)$ of a single particle with an addition term β to correct the effects of neighboring particles. For Ergun-type equation, the parameter α was initially suggested as a function of ϕ in the form of $\alpha(\phi) = b/18(1-\phi)^2$, [9] with b being 1.75 as suggested by Ergun [22]. Later on, it has been realized that F should be optimized in terms of both ϕ and Re, such as the bivariate function of $\alpha(\phi, Re)$ used by Hill et al. [23] and Beetstra et al. [18]. For Wen & Yu-type equation, the corrected term β was initially assumed to be a constant, for example, $\beta = 3.7$ following Wen & Yu [24]. Afterwards, Felice [25] found β is not a constant but has a weak dependency on Re. In fact, Tenneti et al. [26] showed that β can also be estimated via a bivariate functional form $\beta(\phi, Re)$. To sum up, both the Ergun-type and Wen & Yu-type drag formulas can be represented as bivariate functions of ϕ and Re, making them "two-marker" drag models, which means F is essentially associated with ϕ and Re in the homogeneous fluidization systems.

In fact, the effects of closure markers on the performance of drag closures have been investigated by many researchers [27,28]. Except the direct modifications made to the Ergun-type and Wen & Yu-type drag correlations, considering the difference of drag force between a complex fluidized beds system (such as the solids mobility [29–34], heterogeneity [15,35,36], particle inertia [19,37] and so on) and the simple static monodisperse random array system, some researchers have attempted to use a third parameter, in addition to the typical two parameters ϕ and Re, to derive a more accurate drag correlation. The parameters used include granular temperature or solid concentration fluctuation [29–34], particle cluster forming parameter Ha [35], scalar variance of the particle volume fraction $\overline{(\phi')^2}$ and normalized drift flux v_d, [15] heterogeneity index H_i [36], and ratio of the particle relaxation time to fluid relaxation time St [37].

Generally, in fluidized beds, the complex interaction between fluid and particles makes the flow unstable, which can produce the non-uniform multiscale structures [36]. It's very common that individual particles are brought close to each other to form local denser regions of particles [35], especially the particles clusters. These non-uniform multiscale structures can alter the interactions between particles and the fluid and the interactions will differ from that of homogeneous fluidization systems which have been commonly assumed in most CFD modeling works [38]. It's difficult for TFM to achieve grid size convergence with traditional homogeneous drag models due to the existence of heterogeneous structures [39,40], unless a fine enough grid and a small enough time step are used [41], which usually means an expensive computational cost. Especially, for fluidized beds of Geldart A particles in presence of heterogeneous structures, the prediction of flow hydrodynamics using coarse-grid TFM coupling a homogeneous drag model [36] remains a challenge. This issue has become increasingly conspicuous in especially the high-velocity fluidization systems due to the failure of using homogeneous drag models to resolve the mesoscale structures [42]. Although finer grids and smaller time steps can be used to resolve these heterogeneous mesoscale structures, it boosts the computational cost significantly even for lab-scale reactor simulations. So, in large-scale reactor simulations including non-uniform multiscale structures, some heterogeneous drag models have been recently proposed by introducing an extra third parameter based on the traditional "two-marker" homogeneous drag models $F = f(\phi, Re)$. Rubinstein et al. [15] found F can decrease significantly as the extent of inhomogeneities increases over a range of length scales. The extent of inhomogeneities is quantified by the scalar variance of the particle volume fraction or the drift flux which was introduced into drag models as the third parameter. Mehrabadi et al. [35] found the mean drag on clustered configurations decreased compared to that of uniform configurations and proposed a drag model accounting for clusters by introducing the new parameter Ha. Chen et al. [43] found four markers, including the scalar variance of solid volume fraction, the gas drift velocity, the solid drift velocity and a third-order moment, can affect the filtered drag force significantly, and they proposed modified drag models including different combinations of the above four markers. Thus, new parameters accounting for particle concentration configurations are constantly introduced into the traditional "two-marker" homogeneous drag models $F = f(\phi, Re)$ to improve the prediction performance.

Meanwhile, for porous sphere systems, compared with $F = f(Re)$ for solid spheres, permeability which can quantify distributions of particle concentration configurations to some extent is introduced into drag correlations to account for porous structures [7,44,45]. The flow phenomena for flow past these porous structures, are not only depended on the solid fraction, but also related to the detailed internal porous structures [46,47]. Errors occur if the flow is described by porosity alone due to the difference of some related parameters in controlling flow, such as pore size, relative surface area and the space connectivity [48]. So, permeability which is used to correlate the porosity ε ($\varepsilon = 1-\phi$) with associated porous structures [47] is a vital parameter in drag correlations of porous spheres that can quantify with ease for fluid flow past the porous domain [46]. Note that there are similarities in the configurations (such as porosity, monomer sizes and packing ways) between the above two porous systems: monodisperse arrays of spheres and porous spheres. Therefore, drag correlations of them should also be analog and permeability parameters should also have effects on drag correlations of monodisperse arrays of spheres. However, as the authors known, no work has been done to link drag correlations between them.

Meanwhile, it is hard to derive a theoretical expression of drag correlations for either fluidized bed systems or porous spheres at $Re > 0$ due to the existence of theoretical derivation gaps. The rapid development of computer science in recent years makes it now possible to analyze the complex data with theoretical derivation gaps via machine learning methods. One of the effective methods is symbolic regression (SR), which is an advanced computational method for automatically deriving the mathematical expressions by searching both the specific function forms and detailed parameter values simultaneously based on given input–output data. In recent years, SR has been successfully applied to some scenarios in chemical engineering, for example, studying settling velocity of non-cohesive particles [49], predicting voidage distribution in liquid–solid fluidized beds [50], and the establishment of drag correlations for Geldart B particles [8] and for a single solid sphere [51]. However, there is still a gap for considering physical terms of drag correlations in monodisperse arrays of spheres and porous spheres based on SR method.

Support Vector Machine (SVM) is an algorithm for classification based on statistical learning theory [52] to score subsets of variables [53], and can also be an excellent method for feature selection [54].

Therefore, the purpose of our current work is twofold. First, we

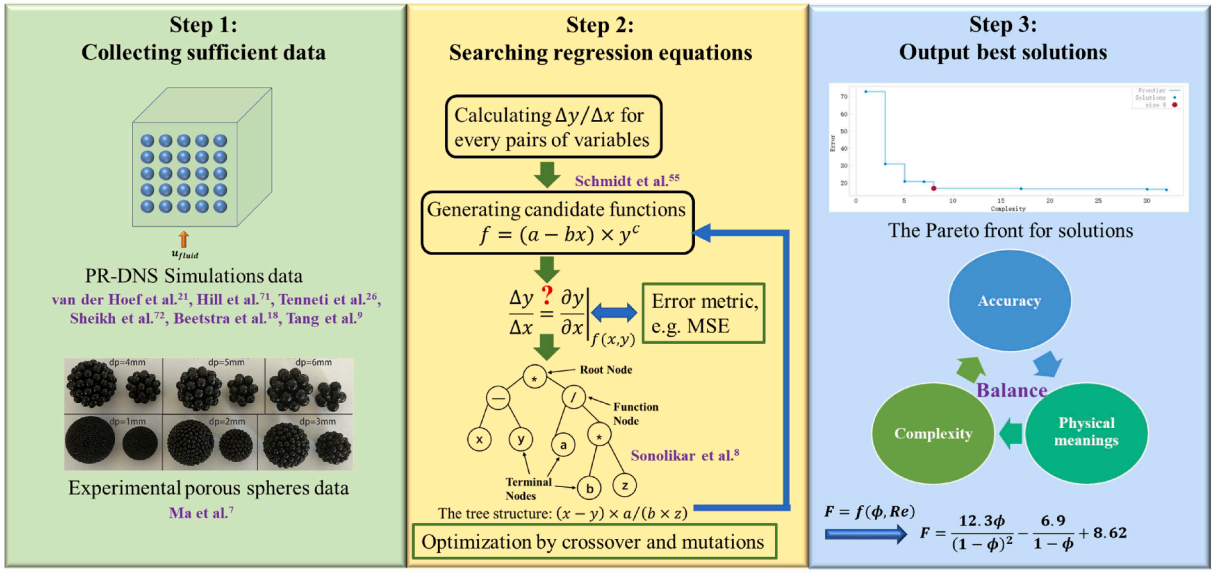

Fig. 1. Flowchart of the symbolic regression approach for generations of drag correlations.

intend to bridge the gap of drag correlations for monodisperse arrays of spheres and porous spheres by considering permeability effects in traditional drag models $F = f(\phi, Re)$. Second, we try to derive new drag correlations accounting for the effects of permeability with physical meanings for flow past monodisperse arrays of spheres and porous spheres using the SR method. The paper is organized as following. We first briefly introduced the SR methodology. Then we used the Support Vector Machine (SVM) to identify the top three important features for drag correlations of porous spheres based on our settling experimental data, followed by the derivation of a drag correlation for porous spheres accounting for the permeability. After that, we analyzed the PR-DNS drag data for flow past random arrays of spheres at small *Re* to confirm the role of permeability in drag correlations. We further obtained a drag correlation for monodisperse arrays of spheres using SR method, which are followed by some discussions and conclusions.

2. Symbolic regression method

Symbolic regression, a supervised machine learning algorithm, is an advanced computational technique that can be used to simultaneously search both specific function forms and optimal parameter values using the available data sets, which allows the derivation of data-fitting function expression forms and parameters with no *in prior* knowledge [8].

Fig. 1 shows the flowchart of SR approach used in this study. Firstly, a set of data are collected. Secondly, the numerical partial derivatives for each pair of variables are calculated and candidate symbolic functions are generated. Symbolic partial derivatives for candidate functions are compared with numerical partial derivatives based on error metrics. Then further optimizations by crossover and mutations are carried out until sufficient accuracy is reached. Therefore, at the final step, best solutions are selected based on the balance of accuracy, complexity and physical meanings. The SR was carried out in this work by use of the software package *Eureqa* developed by Schmidt et al. [55]. All input data sets were split randomly into training data sets and validation data sets, which account for 75% and 25% of whole datasets, respectively, to improve the generality of target equations and avoid overfitting in SR operations [49]. All solutions were evaluated against the Mean Squared Error (MSE), which is the average squared difference between outputs and targets, as defined in Eq. (1), and the Normalized Root Mean Squared Error (NRMSE) as defined in Eq. (2). NRMSE is the normalized MSE, which can eliminate the effect of original data and provide a quantitative criterion for the prediction ability of different correlations:

$$MSE = \frac{1}{n}\sum_{t=1}^{n}(b_t - p_t)^2 \tag{1}$$

$$NRMSE = \sqrt{MSE}/\bar{b} \tag{2}$$

where n is the size of the sample, p the predicted value, b the observed value, and $\bar{b}$ the average of observed values [49].

Formula building blocks used in this study include constants, integer constant, variables and mathematical operators such as addition, subtraction, multiplication, division, exponential, natural logarithm, power and square root. For each formula building block, a specific value was set to examine the complexity of the formula forms [55]. SR was then carried out by finally reaching a trade-off between complexity and accuracy in searching for an optimal solution for formula forms of drag correlations. The total complexity of a solution can be quantified and compared by calculating the sum of complexity for all formula building-blocks in the solution. The search algorithm compares partial derivatives for pairs of variables $\Delta x/\Delta y$ (x and y indicating F, Re and ϕ) obtained from training dataset with symbolic partial derivatives of pairs of variables $\delta x/\delta y$ calculated from each candidate symbolic function $f(x, y)$ to evaluate the prediction ability of intrinsic relations between variables and data, which is detailed in Schmidt et al [55]. The partial-derivative-pairs search criteria can generate a few analytical expressions directly from training data. Some of candidate solutions that can minimize MSE based on validation dataset are reserved while poor performing candidate solutions are discarded [49]. Reserved solutions will have a further evolution and optimization by crossover and mutations and the detailed description can be found in Sonolikar et al [8].

In this study, the termination of SR operation was set as 10^{11} formulas had been generated and evaluated, ensuring the candidate solutions captured as many as possible the key features of data sets. The final output was a series of best solutions with the least error metric and reasonable complexity, and the best correlation was picked manually from the best solutions based on the balance of complexity, accuracy and physical meaning [56].

3. Results and discussions

3.1. Drag correlations for porous spheres

In order to investigate drag correlations of fluidized beds with

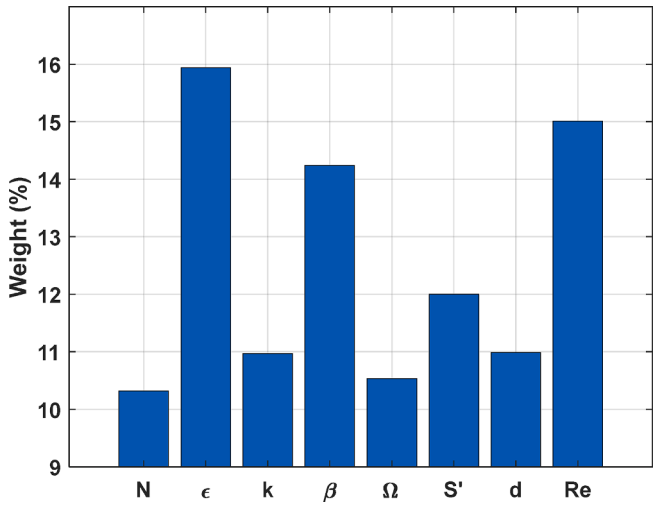

Fig. 2. Weighted ranking of eight features for porous spheres.

spherical clusters existing in a direct experimental way, porous spheres settling experiments were carried out and the details can be found in our previous work [7]. Without incorporating any *in prior* information, 36 experimental drag data sets for porous spheres with $Re = 1 \sim 110$ were used to distill drag correlations of porous spheres. In doing so, the top three most important variables dominating the drag correlations of porous spheres were first selected by SVM method. Then the drag correlations were distilled based on these three variables using SR method.

Many researches have been conducted to link the structural features of a porous domain to permeability k, and thus $k(\phi)$ should be specified for the structure of any given porous solid [57–61]. The permeability model that is the most widely used for a dense sphere-packed swarm is the Carman-Kozeny model [47,59]. It can be expanded into a more common form of $k = \left(\varepsilon^3(d/2)^2\right)/\left(9C(1-\varepsilon)^2\right)$ for hard monodisperse spheres systems of diameter d[62]. It was [47] found the empirical scaling factor $C = 5$ showed a good fit to $k(\phi)$ and is suitable for many porous structures. Thus, $k = \left(\varepsilon^3 d^2\right)/\left(180(1-\varepsilon)^2\right)$ is used to characterize the permeability of monodisperse random array spheres systems in this work. In this work, the normalized permeability β, which is a function of not only the solid concentration ϕ but also the relative dimension d/D, is used to represent permeability property [44,63]. β is calculated by.

$$\beta = D/\left(2\sqrt{k}\right) = D/\left(2\sqrt{(d^2\varepsilon^3)/(180(1-\varepsilon)^2)}\right) \tag{3}$$

where D is the characteristic length of porous domain.

Here, eight input variables of porous spheres, including number of monomers N, porosity ε ($\varepsilon = 1-\phi$), permeability k, dimensionless permeability β, correction factor Ω [64], relative surface area S^* [65], diameter of monomers d and the Reynolds numbers Re (The definition is based on the diameter of the whole porous sphere), together with one output variable, i.e. the drag coefficient C_D, are used to learn feature weights in kernel spaces based on SVM [54]. All features are ranked in Fig. 2 and the results show that ε, Re and β are the top three most important variables which suggests that the normalized permeability should be included in the drag correlations in addition to ε and Re.

Thus, ϕ, Re and β are used as input variables to distill symbolic regression drag correlations of porous spheres and one candidate from the list of Best Solutions is shown as.

$$F = 1.305 + \frac{1.226Re}{24} - \frac{21.06\varepsilon}{24Re} - \frac{17.85Re}{24\beta} \tag{4}$$

As is well known, for a single solid sphere, the common functional form of drag correlations is $F = 1 + f(Re^m)$, with 1 being the Stokes term and $f(Re^m)$ being the additional correction terms for inertial effect at high Re. It is interesting to note that Eq.(4) approximately satisfies the functional form $F = 1 + f(Re^m) + f(Re, \phi, \beta)$, in which the first term 1.305 denotes the Stokes solution for $Re = 0$ and the deviation from the theoretical limit of 1 could be caused by the surface roughness of porous spheres. The second term denotes the correction of inertial effects for $Re > 0$ and the remained term $f(Re, \phi, \beta)$ is the correction term for porous structures. Note that $C_D = (24/Re)F$, we can rewrote the first term $F = 1.305$ as $C_D \sim 31.32/Re$ for the Stokes flow in the limit of $Re \sim 0$, which is quite close to the analytical solution [66], $F = 1$ as well as $C_D \sim 24/Re$. The difference may be due to the nonideal sphericity of the porous spheres compared to that of the solid sphere. It was similarly found that the drag coefficient of a rising spherical bubble with deformations may differ from that of an ideal spherical bubble [67].

Besides, in terms of prediction performance, Eq.(4) can cover all raw data points and characterize major features of raw data points. As shown in Fig. 3(a), most of the relative errors are within ± 15%. The error metrics Mean Relative Error (MRE) and NRMSE of the predicted F by Eq. (4) are respectively 8.83% and 0.266.

Additionally, Eq.(4) can be reasonably reduced to the case of a single solid sphere.

$$F = 1.305 + \frac{1.226Re}{24} \tag{5}$$

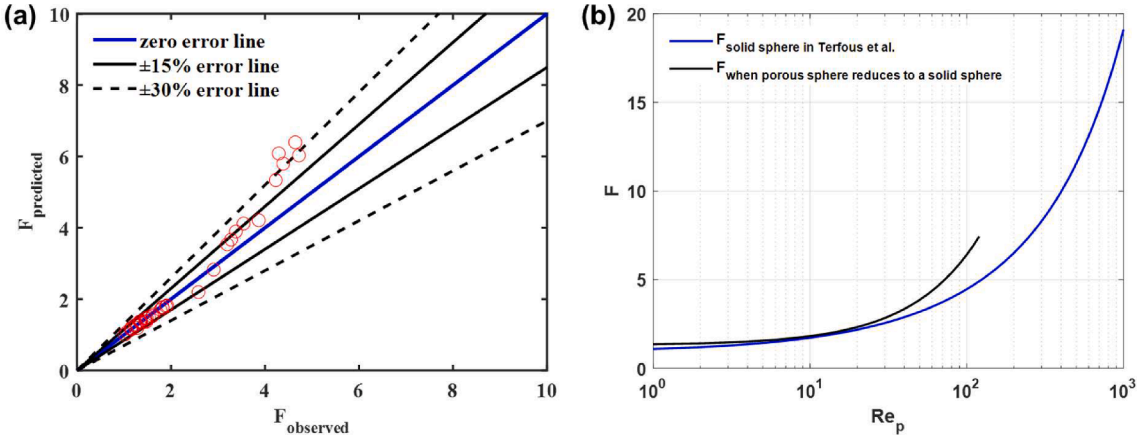

Fig. 3. (a) Comparison of predicted vs. observed F based on Eq.(4), (b) Drag correlations reduced to a single solid sphere for Eq.(5) and drag correlations for a single solid sphere in Terfous et al. [68].

Table 1
Summary of two SR cases for drag correlations at Re = 0

No.	Application range	Target expression	Type
Case 1	$Re = 0$	$F = f(\phi, Re)$	Without prior form
Case 2	$Re = 0$	$F = \frac{10\phi}{(1-\phi)^2} + f(\phi)$	With prior form: Carman theoretical term

by assuming $\varepsilon = 0$ and $\beta \to +\infty$. As shown in Fig. 3(b), the comparison of drag correlations for solid spheres proposed by Terfous et al. [68] with Eq.(5) obtained by SR in this work demonstrates a fairly good agreement, indicating that Eq.(4) can be successfully reduced to the case of a single solid sphere.

3.2. Drag correlations for monodisperse arrays of spheres

Particle-resolved direct numerical simulation (PR-DNS) [69] has been considered as a first principle simulation approach to derive or verify drag correlations for gas–solid systems, because it can calculate the drag force directly by imposing no-slip boundary conditions at the surface of solid particles [35,70]. In most of the PR-DNS simulations, the monodisperse arrays of spheres were taken as the model system for calculating the drag force acting on single particle in presence of surrounding particles with a regular and/or random arrangement. The monodisperse arrays of spheres, to certain extend, manifest similarity to the porous sphere in terms of porous structure. In this work, drag data for monodisperse arrays of spheres from PR-DNS were collected from the literature, which were first used to validate the reasonability of SR method to distill drag correlations underlying discrete drag data points. We then used SR method to develop a new drag correlation by including the permeability for calculating the drag force acting on a single particle in the monodisperse arrays of spheres for a wide range of *Re*.

3.2.1. Validation of SR method for monodisperse arrays of spheres

In this work, 43 drag data points $F = f(\phi, Re)$ directly obtained by PR-DNS for $Re = 0$ from 4 open sources, including van der Hoef et al. [21], Hill et al. [71], Tenneti et al. [26] and Sheikh et al. [72], have been used to automatically derive drag correlations for monodisperse arrays of spheres for Stokes flow via SR method. In SR methods, it is possible to use the prior knowledge to seed equation searching by initializing the search space of candidate formula forms with terms based on known physical information. Two different cases were studied using SR method with or without prior physical information as initial inputs constraining the search space of formula forms. The results are listed in Table 1. Target expressions stated in Table 1 are formula forms used for initial search settings: "without prior form" means that there was no restriction on target expressions and search results were entirely driven by data without any prior knowledge; "prior form" means that a known expression was given *in prior* and algorithms would obtain remaining forms based on the training data. The prior form is Carman equation, which is theoretically derived for $Re = 0$ [21].

Final best solutions for two cases, as well as their range of applicability, accuracy evaluation indexes (MSE, NRMSE, R^2, *CC*), the number of fitting coefficients and complexity values for formula building-blocks, are listed in Table 2. Note that R^2 is the goodness of fit and *CC* is the correlation coefficient, both being evaluated against validation data. $N_{fitting}$ and *C* are respectively the number of fitting coefficients and the complexity, which are statistical values based on the searched forms excluding the pre-defined forms.

As shown in Table 2, without incorporating any *in prior* knowledge, the best solution for Case 1 includes the same theoretical term $F = 2k \times \phi/(1-\phi)^2$ derived by Carman [20], which illustrates that the intrinsic relationship between *F* and ϕ underlying the collected data sets can be captured.

SR regression equations can also satisfy reasonable limiting values. For case 2, incorporated in prior information in SR operation, the Carman equation $F = 10\phi/(1-\phi)^2$ was assumed as a feature term and the Best Solution 2 can reduce to $F = 1$ as ϕ approaches 0, which reflects drag force of a single solid sphere in Stokes flow. Due to the nonideality of collected data sets, the Best Solution 1, which was derived without any in prior information, have a slight bias with $F(\phi = 0, Re = 0) = 1$. The existence of such small deviation is probably due to the pathological nature in mathematics for fitting nonideal data points with noises.

Besides, as shown in Fig. 4(a), NRMSE for both the Best Solutions 1 and 2 are smaller than that of the correlation in van der Hoef et al [21], which is the "most accurate" drag correlation for $Re = 0$ system for static monodisperse random arrays so far. It indicates that SR has the better prediction accuracy for obtaining drag correlations, even when the size

Table 2
Best solutions of two SR cases for drag correlations at Re = 0

Case	Best Solution	Application range	MSE & NRMSE	R^2&*CC*	$N_{fitting}$&*C*
1	$F = \frac{12.3\phi}{(1-\phi)^2} - \frac{6.9}{1-\phi} + 8.62$	$Re = 0, \quad \phi = [0, 0.71]$	0.846 0.049	$R^2 = 0.995$ $CC = 0.998$	3 13
2	$F = \frac{10\phi}{(1-\phi)^2} + (1-\phi)\sqrt{1-\phi}$	$Re = 0, \quad \phi = [0, 0.71]$	1.969 0.074	$R^2 = 0.992$ $CC = 0.996$	0 7

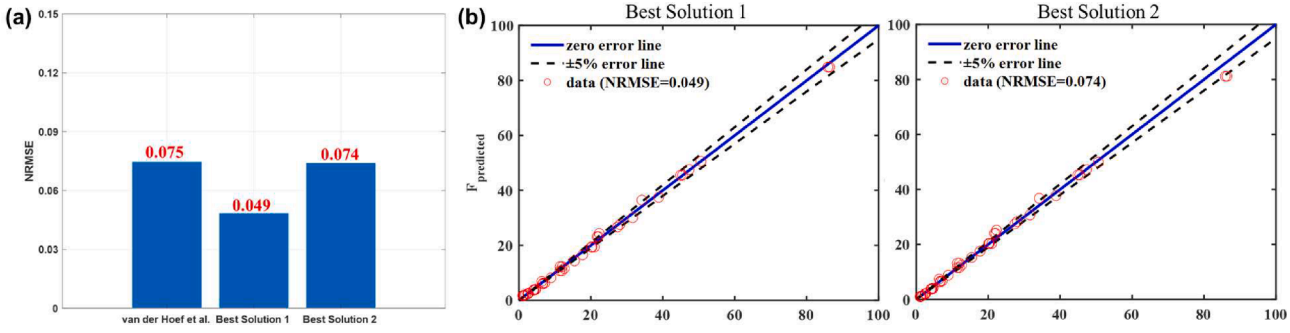

Fig. 4. (a) Comparison of NRMSE for Best Solutions 1, 2 and van der Hoef et al [21], (b) predicted vs. observed F for Best Solutions 1 and 2.

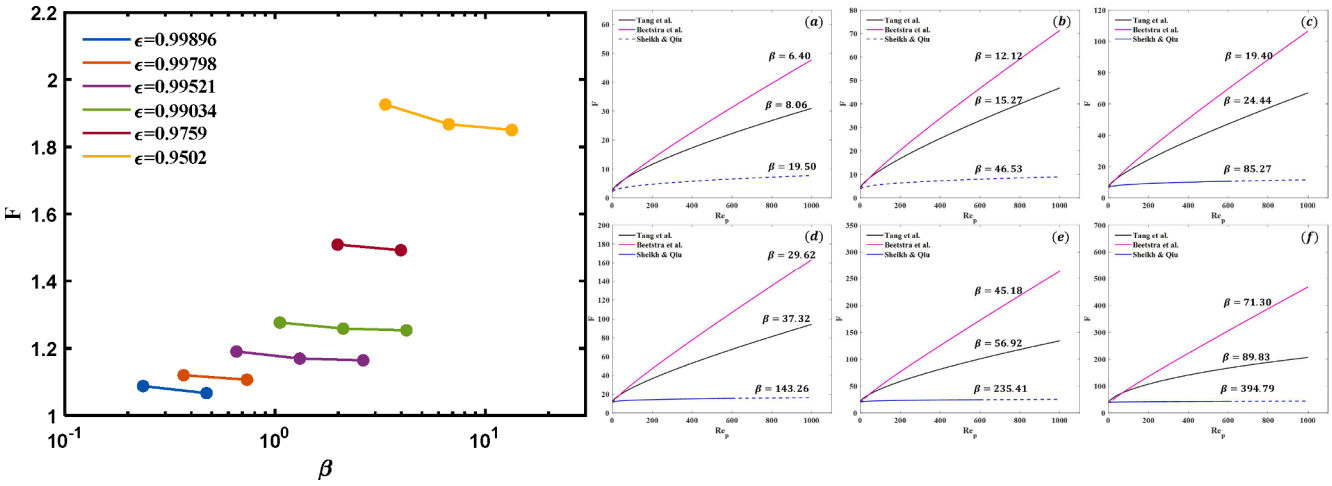

Fig. 5. Variation of F along β at different porosity ε for Re = 0 in Hill et al. [71] (left), (b) The difference of simulated F as a function of Re for different authors in the literature for $0 \le Re < 1050$ (right): (a)ϕ = 0.1, (b)ϕ = 0.2, (c)ϕ = 0.3, (d)ϕ = 0.4, (e)ϕ = 0.5, (f)ϕ = 0.6.

of data set is as small as only 43 data points. In addition, the predicted F versus the observed one for the Best Solutions 1 and 2 are plotted in Fig. 4(b). The relative errors for SR derived correlations are within ± 5%.

All assessed SR correlations, without any negative or other abnormal values (outliers or mutant values), manifest a consistent trend with existing correlations (Carman [20], Kim & Russel [73], Ergun [22], Wen & Yu [24], van der Hoef et al. [21], Tang et al. [9], Tenneti et al. [26], Beetstra et al. [18], Hill et al. [23], Brinkman [21], Koch & Sangani [74]) and data points (van der Hoef et al. [21], Hill et al. [23], Tenneti et al. [26], Sheikn & Qiu [72]) in the literature. Thus, the output F can be a good approximation in the parameters space if the input ϕ and Re are reasonably chosen.

Additionally, one of the most important applications of drag correlations is to calculate the interphase momentum transfer in CFD simulations for solid–gas two-phase flows. Therefore, the continuity of the first and second derivatives of F over ϕ are quite essential to ensure the numerical stability of CFD simulations. The first derivative $\partial F/\partial\phi$ and the second derivative $\partial^2 F/\partial^2\phi$ for Best Solutions 1 and 2 are continuous, smooth and nonconstant over the whole range of ϕ, which indicates them can be potentially used in CFD simulations.

Thus, after the successfully validation, it can be regarded that SR can distill the physics and relationships underlying discrete drag data points. The permeability parameter will be introduced into drag correlations for monodisperse arrays of spheres in the following section.

3.2.2. New drag correlations with β for monodisperse arrays of spheres

DNS for flow past monodisperse random array spheres of diameter d in fluidization system are usually carried out in a box of $n_x \times n_y \times n_z$ lattice sites with a specific number of particles N [9,18,21,71]. So, the correlation between solid fraction, particle number and box size is written as Eq.(6).

$$\phi = N\pi d^3/\left(6n_x n_y n_z\right) \tag{6}$$

The cubic box is transformed to an equivalent diameter D of a sphere and when ϕ and N are given, d/D can be obtained by Eq.(6). Then, the dimensionless permeability β can be calculated based on Eq.(3) with a given ϕ.

For $Re = 0$, in Hill et al. [71], simulation parameters used for simulations of Stokes flow in monodisperse random array spheres are given and we calculated the dimensionless permeability β based on each ϕ. Hill et al. [71] found F is inversely proportional to N which is the number of spheres in their computational domain. A prior equation form $F = k_1(\phi) + k_2 N^{-1}$ was given for $Re = 0$ and fitted to plots based on two markers ϕ and N in their work, written as $F = 1 + \left(3/\sqrt{2}\right)\phi^{1/2} + 0.667N^{-1}$. In this work, β was further calculated by us based on N, ϕ and Eq.(6) and it was found that F decreased with β increasing at a same porosity, as Fig. 5(a) shown, which indicated that permeability indeed has effects on the simulated drag force F for $Re = 0$.

For $Re > 0$, as can be seen from Fig. 5(b), when ϕ and Re are the same, it is clear that there is a difference among the simulated F for different authors [9,18,72] due to the different permeability depended on their computational domain settings. According to the β that are calculated based on parameters of computational domains in the literature [9,18,72], it can be found that F are also inversely proportional to β for $Re > 0$.

Thus, in this section, based on ϕ, Re as well as β, we further explore the feasibility of using SR to obtain a new three-parameter drag correlations accounting for the effect of permeability for monodisperse arrays of spheres. Following the SR method in Section 2, without incorporating any prior information or prior formula forms, we distilled 221 PR-DNS data for $0 \le Re < 1050$ for monodisperse arrays of spheres in Hill et al. [71], Beetstra et al. [18], Tang et al. [9] and Sheikh and Qiu [72] in which parameters of computational domain to calculate permeability were provided. One correlation from the list of Best Solutions is shown here:

$$F = \frac{8.44\phi}{(1-\phi)^2} + \frac{8.44\phi}{(1-\phi)} + \frac{0.889}{(1-\phi)^2} + \frac{0.03842Re - 6.494\times10^{-6}Re^2}{(1-\phi)^2} + \left(\frac{0.0001212Re\times\beta}{(1-\phi)^2} + \frac{0.214\beta}{(1-\phi)\sqrt{Re} - 32.1(1-\phi)}\right) \tag{7}$$

It is interesting to note that Eq.(7) satisfies the functional form $F = 2k\times\phi/(1-\phi)^2 + f(\phi) + f(\phi,Re) + f(\phi,Re,\beta)$, in which the first term $2k\times\phi/(1-\phi)^2 = 8.44\phi/(1-\phi)^2$ denotes the theoretical term derived by Carman [20] for $Re = 0$, the second term $f(\phi) = 8.44\phi/(1-\phi) + 0.889/(1-\phi)^2$ represents the correction for stokes limiting case $F(\phi = 0, Re = 0) = 1$ and the third term $f(\phi,Re) = \left(0.03842Re - 6.494\times10^{-6}Re^2\right)/(1-\phi)^2$ is the correction term for inertial effects for high Re regime. The remained term $f(\phi,Re,\beta) = 0.0001212Re\times\beta/(1-\phi)^2 + 0.214\beta/\left((1-\phi)\sqrt{Re} - 32.1(1-\phi)\right)$ is the correction term for permeability effects. It should be stressed that, the CK relation will reduce to Carman equation for $k = 5$ and Ergun equation for $k = 4.167$. We argued that the reasonable range of empirical coefficients $2k$ is $8.334 \sim 10$ which covers the coefficient 8.44 in the first term in Eq.(7), indicating the reasonability of the first fitting term. For stokes limiting case, Eq.(7) comes to $F(\phi = 0, Re = 0) =$

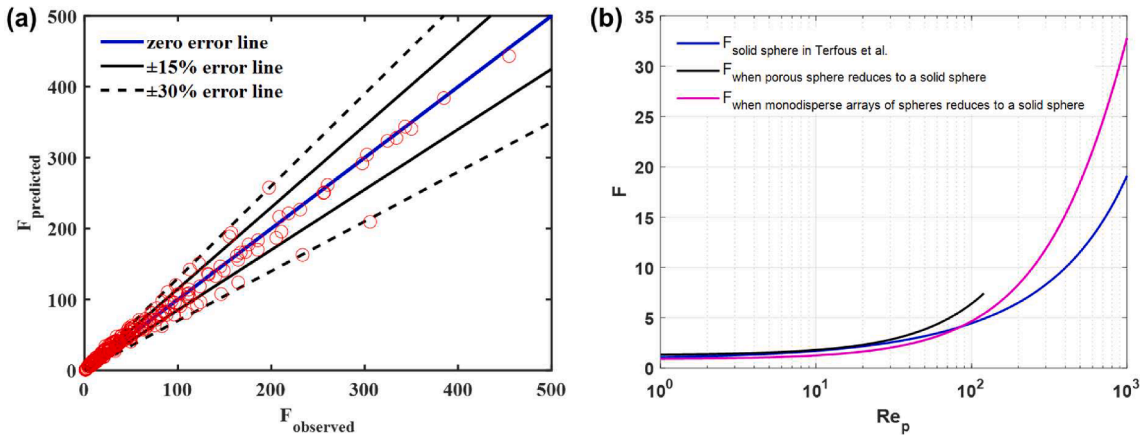

Fig. 6. (a) Comparison of predicted vs. observed F based on Eq.(7), (b) Drag correlations reduced to a single solid sphere for Eq.(5), Eq.(11) and drag correlations for a single solid sphere in Terfous et al. [68].

0.889 which is very close to the theoretical value 1, which also proves the SR method can unveil the underlying physics reasonably. Eq.(7) can cover all raw data points and characterize major features of raw data points with a low error metrics MRE = 14.1% and NRMSE = 0.182, indicating a good prediction performance. As shown in Fig. 6(a), most of the relative errors are within ± 30%.

Eq.(7) can be reduced to a reasonable bivariate functional form $F = f(\phi,\beta)$ for stokes flow at the limit of $Re = 0$:

$$F = f(\phi,\beta) = \frac{8.44\phi + 0.889}{(1-\phi)^2} + \frac{8.44 * \phi}{(1-\phi)} - \frac{0.214\beta}{32.1(1-\phi)} \tag{8}$$

In Hill et al [71], as mentioned above, for $Re = 0$, it was found that F is inversely proportional to N, which is the number of spheres in the computational domain and a fitting correlation $F = f(\phi, N)$ was given as Eq.(9) shown.

$$F = 1 + \left(3/\sqrt{2}\right)\phi^{0.5} + 0.667N^{-1} \tag{9}$$

Eq.(9) can be further written as $F = f(\phi,\beta)$, as shown in Eq.(10), in order to be compared with our results in Eq.(8).

$$F = 1 + \left(3/\sqrt{2}\right)\phi^{0.5} + 0.667\left(\frac{6\phi}{\pi} \times \left(\frac{45\phi^2}{\beta^2(1-\phi)^3}\right)^{-1.5}\right)^{-1} \tag{10}$$

It can be found that the error metric of the predicted F by Eq.(8) is MRE = 23.7% and NRMSE = 0.540 which are still much lower than that (MRE = 40.0%, NRMSE = 1.545 based on Eq.(10)) in Hill et al [71], which indicates the prediction accuracy is improved significantly even when Eq.(7) is reduced to Stokes flow.

Additionally, Eq.(7) can also correctly reduce to a single solid sphere case when $\beta \to 0$ by assuming $\phi \to 0$ and $k \to +\infty$, i.e. in case of the void. Eq.(7) can be written as Eq.(11).

$$F = 0.889 + 0.03842Re - 6.494 \times 10^{-6}Re^2 \tag{11}$$

As shown in Fig. 6(b), the proposed drag correlation Eq.(7) can also reduce to a single solid sphere successfully. The agreement of Eq.(5), Eq.(11) and drag correlations for a single solid sphere in Terfous et al. [68] in Fig. 6(b) indicates when it is reduced to a single solid sphere, drag correlations for monodisperse arrays of spheres and porous spheres can achieve approximately the same results.

Note that it is a common practice to give a prior equation form by manual interferences to satisfy the physics considerations/limiting cases and to fit the remained terms using experiments/simulations data in deriving drag correlations. As can be found here, without any prior knowledge or expression forms, drag correlation Eq.(7) obtained by SR method based on the open sources PR-DNS data can automatically account for the effect of permeability with physical basis. Additionally, it can both correctly reduce to drag correlations for a single solid sphere and/or stokes flow at the limit of $Re = 0$. Owing to the data-driven nature, Eq.(7) agrees satisfactorily with original data points with a low error metrics MRE and NRMSE, which suggests that the data-driven drag correlation derived using SR method is robust and generic.

4. Conclusions

This work provides a way to bridge the gap of drag correlations for monodisperse arrays of spheres in fixed beds and porous spheres in fluidized beds by introducing parameters of permeability into drag correlations. New drag correlations are generated by data driven based on symbolic regression method without any prior target expression.

For porous spheres, the top three most important features ϕ, Re, β are picked up by Support Vector Machine method based on our experimental porous sphere drag data which verifies the importance of permeability effect in porous sphere systems. Then, based on the above three parameters, a drag correlation $F = f(\phi, Re, \beta)$ which has physics, high prediction accuracy and correct limiting cases, is automatically generated by symbolic regression.

For monodisperse arrays of spheres, by use of the PR-DNS drag data points available in open sources, we found that permeability indeed has effects on the simulated drag force F. With 221 PR-DNS data for $0 \leq Re < 1050$ collected, we derived a new three-parameter drag correlation $F = f(\phi, Re, \beta)$ using SR method, which was based on the same three parameters as those of porous spheres, introduced the dimensionless permeability β as the third parameter into traditional drag correlations. It is shown that the derived three-parameter drag correlation has solid physical basis, good prediction performance and correct limiting cases when reduced to a single solid sphere [68] and/or Stokes flow at $Re = 0$.

It is further shown that for the limiting case of reducing to a single solid sphere, drag correlations for monodisperse arrays of spheres and porous spheres can reach a state of unity. Thus, new drag correlations are introducing permeability parameters into traditional drag models $F = f(\phi, Re)$. On the one hand, it might be possible to use permeability as a simple yet physically sounded parameter for understanding the heterogeneous structures in fluidized beds. On the other hand, it could provide a way to link drag correlations for monodisperse arrays of spheres and porous spheres, which may open a venue for directly validating the drag correlations obtained purely from CFD simulations with experimental data of the fluid flow around porous spheres.

Declaration of Competing Interest

The authors declare that they have no known competing financial

interests or personal relationships that could have appeared to influence the work reported in this paper.

Acknowledgments

This work is part of a research program financially supported by the National Natural Science Foundation of China under Grant No. 21991093 and 91834302.

Appendix A. Supplementary data

Supplementary data to this article can be found online at https://doi.org/10.1016/j.cej.2022.136653.

References

[1] D.P. Haughey, G.S.G. Beveridge, Structural properties of packed beds - A review, The Canadian Journal of Chemical Engineering 47 (2) (1969) 130–140.
[2] J. Wang, J. Yang, Z. Cheng, Y. Liu, Y. Chen, Q. Wang, Experimental and numerical study on pressure drop and heat transfer performance of grille-sphere composite structured packed bed, Appl. Energy 227 (2018) 719–730.
[3] T. Claes, T.V. Gerven, M.E. Leblebici, Design considerations for photocatalytic structured packed bed reactors, Chem. Eng. J. 403 (2021) 126355.
[4] A. Cahyadi, A. Anantharaman, S. Yang, S.B.R. Karri, J.G. Findlay, R.A. Cocco, J. W. Chew, Review of cluster characteristics in circulating fluidized bed (CFB) risers, Chem. Eng. Sci. 158 (2017) 70–95.
[5] X. Wei, Experimental Investigations on the Instantaneous Flow Structure in Circulating Fluidized Beds, Electronic Thesis and Dissertation Repository. 6164 (2019). https://ir.lib.uwo.ca/etd/6164.
[6] P. Yu, Y. Zeng, T.S. Lee, X.B. Chen, H.T. Low, Numerical simulation on steady flow around and through a porous sphere, Int. J. Heat Fluid Flow 36 (2012) 142–152.
[7] L. Ma, S. Xu, X. Li, Q. Guo, D. Gao, Y. Ding, M. Ye, Z. Liu, Particle tracking velocimetry of porous sphere settling under gravity: Preparation of the model porous particle and measurement of drag coefficients, Powder Technol. 360 (2020) 241–252.
[8] R.R. Sonolikar, M.P. Patil, R.B. Mankar, S.S. Tambe, B.D. Kulkarni, Genetic Programming based Drag Model with Improved Prediction Accuracy for Fluidization Systems, Int. J. Chem. Reactor Eng. 15 (2) (2017) 20160210.
[9] Y. Tang, E.A.J.F. Peters, J.A.M. Kuipers, S.H.L. Kriebitzsch, M.A. van der Hoef, A new drag correlation from fully resolved simulations of flow past monodisperse static arrays of spheres, AIChE J. 61 (2) (2015) 688–698.
[10] K. Agrawal, P.N. Loezos, M. Syamlal, S. Sundaresan, The role of meso-scale structures in rapid gas–solid flows, J. Fluid Mech. 445 (2001) 151–185.
[11] B.G.M. van Wachem, J.C. Schouten, C.M. van den Bleek, R. Krishna, J.L. Sinclair, Comparative analysis of CFD models of dense gas–solid systems, AIChE J. 47 (5) (2001) 1035–1051.
[12] X. Liu, W. Ge, L. Wang, Scale and structure dependent drag in gas–solid flows, AIChE J. 66 (4) (2020), e16883.
[13] J. Wang, Continuum theory for dense gas-solid flow: A state-of-the-art review, Chem. Eng. Sci. 215 (2020) 115428.
[14] D. Kandhai, J.J. Derksen, H.E.A. Van den Akker, Interphase drag coefficients in gas-solid flows, AIChE J. 49 (4) (2003) 1060–1065.
[15] G.J. Rubinstein, A. Ozel, X. Yin, J.J. Derksen, S. Sundaresan, Lattice Boltzmann simulations of low-Reynolds-number flows past fluidized spheres: effect of inhomogeneities on the drag force, J. Fluid Mech. 833 (2017) 599–630.
[16] L.T. Zhu, J.X. Tang, Z.H. Luo, Machine learning to assist filtered two-fluid model development for dense gas–particle flows, AIChE J. 66 (6) (2020), e16973.
[17] L.-T. Zhu, X.-Z. Chen, Z.-H. Luo, Analysis and development of homogeneous drag closure for filtered mesoscale modeling of fluidized gas-particle flows, Chem. Eng. Sci. 229 (2021) 116147.
[18] R. Beetstra, M.A. van der Hoef, J.A.M. Kuipers, Drag force of intermediate Reynolds number flow past mono- and bidisperse arrays of spheres, AIChE J. 53 (2) (2007) 489–501.
[19] A.A. Zaidi, Study of particle inertia effects on drag force of finite sized particles in settling process, Chem. Eng. Res. Des. 132 (2018) 714–728.
[20] P.C. Carman, Fluid flow through granular beds, Trans IChemE 15 (1937) S32–S48.
[21] M.A.V.D. Hoef, R. Beetstra, J.A.M. Kuipers, Lattice-Boltzmann simulations of low-Reynolds-number flow past mono- and bidisperse arrays of spheres: results for the permeability and drag force, J. Fluid Mech. 528 (2005) 233–254.
[22] S. Ergun, Fluid Flow through Packed Columns, Chem. Eng. Prog. 48 (2) (1952) 89–94.
[23] R.J. Hill, D.L. Koch, A.J.C. Ladd, Moderate-Reynolds-number flows in ordered and random arrays of spheres, J. Fluid Mech. 448 (2001) 243–278.
[24] C.Y. Wen, Y.H. Yu, Mechanics of fluidization, AIChE J. 62 (1966) 100–111.
[25] R. Di Felice, The voidage function for fluid-particle interaction systems, Int. J. Multiph. Flow 20 (1) (1994) 153–159.
[26] S. Tenneti, R. Garg, S. Subramaniam, Drag law for monodisperse gas–solid systems using particle-resolved direct numerical simulation of flow past fixed assemblies of spheres, Int. J. Multiph. Flow 37 (9) (2011) 1072–1092.
[27] L.T. Zhu, Y.X. Liu, J.X. Tang, Z.H. Luo, A material-property-dependent sub-grid drag model for coarse-grained simulation of 3D large-scale CFB risers, Chem. Eng. Sci. 204 (2019) 228–245.
[28] L.T. Zhu, B. Ouyang, H. Lei, Z.H. Luo, Conventional and data-driven modeling of filtered drag, heat transfer, and reaction rate in gas–particle flows, AIChE J. 67 (8) (2021), e17299.
[29] J.J. Wylie, D.L. Koch, A.J.C. Ladd, Rheology of suspensions with high particle inertia and moderate fluid inertia, J. Fluid Mech. 480 (2003) 95–118.
[30] Y. Zhang, J.M. Reese, The drag force in two-fluid models of gas–solid flows, Chem. Eng. Sci. 58 (8) (2003) 1641–1644.
[31] Y. Tang, E.A.J.F. Peters, J.A.M. Kuipers, Direct numerical simulations of dynamic gas-solid suspensions, AIChE J. 62 (6) (2016) 1958–1969.
[32] Z. Huang, H. Wang, Q. Zhou, T. Li, Effects of granular temperature on inter-phase drag in gas-solid flows, Powder Technol. 321 (2017) 435–443.
[33] J. Wang, Effect of granular temperature and solid concentration fluctuation on the gas-solid drag force: A CFD test, Chem. Eng. Sci. 168 (2017) 11–14.
[34] W. Bian, X. Chen, J. Wang, Assessment of the interphase drag coefficients considering the effect of granular temperature or solid concentration fluctuation via comparison of DNS, DPM, TFM and experimental data, Chem. Eng. Sci. 223 (2020) 115722.
[35] M. Mehrabadi, E. Murphy, S. Subramaniam, Development of a gas–solid drag law for clustered particles using particle-resolved direct numerical simulation, Chem. Eng. Sci. 152 (2016) 199–212.
[36] X. Gao, T. Li, A. Sarkar, L. Lu, W.A. Rogers, Development and validation of an enhanced filtered drag model for simulating gas-solid fluidization of Geldart A particles in all flow regimes, Chem. Eng. Sci. 184 (2018) 33–51.
[37] G.J. Rubinstein, J.J. Derksen, S. Sundaresan, Lattice Boltzmann simulations of low-Reynolds-number flow past fluidized spheres: effect of Stokes number on drag force, J. Fluid Mech. 788 (2016) 576–601.
[38] J. Wang, A Review of Eulerian Simulation of Geldart A Particles in Gas-Fluidized Beds, Ind. Eng. Chem. Res. 48 (12) (2009) 5567–5577.
[39] Y. Igci, A.T. Andrews, S. Sundaresan, S. Pannala, T. O'Brien, Filtered two-fluid models for fluidized gas-particle suspensions, AIChE J. 54 (6) (2008) 1431–1448.
[40] T. Li, A. Gel, S. Pannala, M. Shahnam, M. Syamlal, CFD simulations of circulating fluidized bed risers, part I: Grid study, Powder Technol. 254 (2014) 170–180.
[41] J. Wang, M.A. van der Hoef, J.A.M. Kuipers, Why the two-fluid model fails to predict the bed expansion characteristics of Geldart A particles in gas-fluidized beds: A tentative answer, Chem. Eng. Sci. 64 (3) (2009) 622–625.
[42] K. Hong, S. Chen, W. Wang, J. Li, Fine-grid two-fluid modeling of fluidization of Geldart A particles, Powder Technol. 296 (2016) 2–16.
[43] X. Chen, N. Song, M. Jiang, Q. Zhou, Theoretical and numerical analysis of key sub-grid quantities' effect on filtered Eulerian drag force, Powder Technol. 372 (2020) 15–31.
[44] J.H. Masliyah, M. Polikar, Terminal velocity of porous spheres, The Canadian Journal of Chemical Engineering 58 (3) (1980) 299–302.
[45] A.K. Jain, S. Basu, Flow Past a Porous Permeable Sphere: Hydrodynamics and Heat-Transfer Studies, Ind. Eng. Chem. Res. 51 (4) (2012) 2170–2178.
[46] R.T. Armstrong, Z. Lanetc, P. Mostaghimi, A. Zhuravljov, A. Herring, V. Robins, Correspondence of max-flow to the absolute permeability of porous systems, Phys. Rev. Fluids 6 (5) (2021), 054003.
[47] J. Vasseur, F.B. Wadsworth, J.P. Coumans, D.B. Dingwell, Permeability of packs of polydisperse hard spheres, Phys. Rev. E 103 (6) (2021), 062613.
[48] C.F. Berg, Permeability Description by Characteristic Length, Tortuosity, Constriction and Porosity, Transp. Porous Media 103 (3) (2014) 381–400.
[49] E.B. Goldstein, G. Coco, A machine learning approach for the prediction of settling velocity, Water Resour. Res. 50 (4) (2014) 3595–3601.
[50] O.J.I. Kramer, J.T. Padding, W.H. van Vugt, P.J. de Moel, E.T. Baars, E.S. Boek, J. P. van der Hoek, Improvement of voidage prediction in liquid-solid fluidized beds by inclusion of the Froude number in effective drag relations, Int. J. Multiph. Flow 127 (2020) 103261.
[51] Hasadi, Y. E.; Padding, J., On the Existence of Logarithmic Terms in the Drag Coefficient and Nusselt Number of a Single Sphere at High Reynolds Numbers. *arXiv preprint arXiv:2007.10214 (2020)*.
[52] C.J. Burges, A tutorial on support vector machines for pattern recognition, Data Min. Knowl. Disc. 2 (2) (1998) 121–167.
[53] C. Zhang, X. Lu, X. Zhang, Significance of gene ranking for classification of microarray samples, IEEE/ACM Trans. Comput. Biol. Bioinf. 3 (3) (2006) 312–320.
[54] Q. Liu, C. Chen, Y. Zhang, Z. Hu, Feature selection for support vector machines with RBF kernel, Artif. Intell. Rev. 36 (2) (2011) 99–115.
[55] M. Schmidt, H. Lipson, Distilling free-form natural laws from experimental data, Science 324 (5923) (2009) 81–85.
[56] M.Y. Liu, W.X. Huai, Z.H. Yang, Y.H. Zeng, A genetic programming-based model for drag coefficient of emergent vegetation in open channel flows, Adv. Water Resour. 140 (2020), 103582.
[57] R.M. Fand, B.Y.K. Kim, A.C.C. Lam, R.T. Phan, Resistance to the Flow of Fluids Through Simple and Complex Porous Media Whose Matrices Are Composed of Randomly Packed Spheres, J. Fluids Eng. 109 (3) (1987) 268–273.
[58] A.S. Kim, R. Yuan, Hydrodynamics of an ideal aggregate with quadratically increasing permeability, J Colloid Interface Sci 285 (2) (2005) 627–633.
[59] Y. Shi, Y.T. Lee, A.S. Kim, Permeability calculation of sphere-packed porous media using dissipative particle dynamics, Desalin. Water Treat. 34 (1–3) (2011) 277–283.
[60] K. Yazdchi, S. Srivastava, S. Luding, Microstructural effects on the permeability of periodic fibrous porous media, Int. J. Multiph. Flow 37 (8) (2011) 956–966.
[61] B. Markicevic, Properties of mono- and poly-disperse spheres random pack media, Powder Technol. 350 (2019) 154–161.

[62] B.R. Corrochano, J.R. Melrose, A.C. Bentley, P.J. Fryer, S. Bakalis, A new methodology to estimate the steady-state permeability of roast and ground coffee in packed beds, J. Food Eng. 150 (2015) 106–116.
[63] K. Wittig, A. Golia, P.A. Nikrityuk, 3D numerical study on the influence of particle porosity on heat and fluid flow, Progress in Computational Fluid Dynamics, An International Journal 12 (2/3) (2012) 207–219.
[64] A.S. Kim, K.D. Stolzenbach, The permeability of synthetic fractal aggregates with realistic three-dimensional structure, J Colloid Interface Sci 253 (2) (2002) 315–328.
[65] K. Wittig, P. Nikrityuk, A. Richter, Drag coefficient and Nusselt number for porous particles under laminar flow conditions, Int. J. Heat Mass Transf. 112 (2017) 1005–1016.
[66] N.S. Cheng, Comparison of formulas for drag coefficient and settling velocity of spherical particles, Powder Technol. 189 (3) (2009) 395–398.
[67] D.D. Joseph, Rise velocity of a spherical cap bubble, J. Fluid Mech. 488 (2003) 213–223.
[68] A. Terfous, A. Hazzab, A. Ghenaim, Predicting the drag coefficient and settling velocity of spherical particles, Powder Technol. 239 (2013) 12–20.
[69] S. Tenneti, S. Subramaniam, Particle-Resolved Direct Numerical Simulation for Gas-Solid Flow Model Development, Annu. Rev. Fluid Mech. 46 (1) (2014) 199–230.
[70] L.T. Zhu, Y.X. Liu, Z.H. Luo, An enhanced correlation for gas-particle heat and mass transfer in packed and fluidized bed reactors, Chem. Eng. J. 374 (2019) 531–544.
[71] R.J. Hill, D.L. Koch, A.J.C. Ladd, The first effects of fluid inertia on flows in ordered and random arrays of spheres, J. Fluid Mech. 448 (2001) 213–241.
[72] B. Sheikh, T. Qiu, Pore-scale simulation and statistical investigation of velocity and drag force distribution of flow through randomly-packed porous media under low and intermediate Reynolds numbers, Comput. Fluids 171 (2018) 15–28.
[73] S. Kim, W.B. Russel, Modelling of porous media by renormalization of the Stokes equations, J. Fluid Mech. 154 (1985) 269–286.
[74] D.L. Koch, A.S. Sangani, Particle pressure and marginal stability limits for a homogeneous monodisperse gas-fluidized bed: kinetic theory and numerical simulations, J. Fluid Mech. 400 (1999) 229–263.